A Physics-Based Continuous Charge-Sheet MOSFET Model Using a Balanced Bulk-Charge-Sharing Method

S. D. Cho, H. T. Kim, S. J. Song, S. S. Chi, M. S. Kim, W. S. Chang,
H. J. Kang, H. T. Shin, T. E. Kim, D. J. Kim and D. M. Kim*

School of Electrical Engineering, Kookmin University, Seoul 136-702

In this paper, we propose a new physics-based charge-sheet model for submicrometer MOSFETs for circuit simulation. Based on solving a balanced bulk charge sharing method and the transport equation, proposed model provides physical insights into the current-voltage behavior describing continuous and unified current characteristics of MOSFETs from the subthreshold to strong inversion regions as well as from the linear to the saturation regions. In particular, discontinuities in the second derivative, at the electrical boundary between forward- and reverse-mode operations and vice versa of I-V characteristics, which are usual in other previous MOSFET models, are significantly improved. These advantages are obtained by averaging the bulk charge and effective channel carrier mobility models over the channel length with respect to the source- and drain-end surface potentials. The resulting MOSFET model also satisfies the Gummel symmetry test which is a requirement for a bi-directional signal flow in the design of high performance digital integrated circuits with MOSFETs. Comparison with measured data is presented to verify the new model in which the model parameters are extracted efficiently by simple and accurate methods.

I. INTRODUCTION

With a fast development of MOS ULSI technology to implement high performance digital and mixed analog-digital signal processing and low voltage operation, circuit designers require accurate and continuous Metal-Oxide-Semiconductor Field Effect Transistor (MOSFET) model for use in circuit simulators. An accurate modeling of small geometry MOSFETs requires the numerical solution of two- or three-dimensional Poisson's equation and current continuity equation. However, time-consuming numerical calculations are not quite suitable for the circuit design and simulation which require analytical models with as small number of empirical parameters as possible, nor for the rapid characterization of process parameters. For example, the earliest models such as the SPICE level 1 and level 2 models were highly empirical and contained discontinuities in their current and capacitance characteristics so that they did not conserve charge or incorporate the physics of small geometry devices accurately. Therefore an analytical MOSFET model should combine the accuracy with a relative simplicity of the formulation [1–10].

Conventional MOSFET models have been successfully used for the long-channel devices. However, the scaling down of MOSFETs to a deep submicrometer regime leads to deviations from assumptions in the conventional models, which include the gradual channel approximation (GCA), the hole current in n-MOSFETs, the generation and recombination rate in the channel, the direction of the current flow, and the effective mobility in the channel [4, 5]. Moreover, most widely adopted BSIM3v3 model is also derived based on the source-referenced model with smoothing functions which has discontinuities in the derivatives of the drain current and terminal charges at the boundary between forward and reverse mode operation. These discontinuities arise primarily from the use of the source as a reference terminal for the potential, the velocity-field expressions, and the smoothing functions used in the transition area between the linear and saturation regions. These deficiencies affect the accuracy in the simulation of higher order effects, such as amplifier distortion and the convergence rate of transient simulations, in analog and communication circuits [5,6].

As a solution to the above issue, we propose a physics-based continuous charge-sheet model which is continuous over all operation regions, of linear, saturation, and subthreshold regimes. The bulk charge density in the balanced bulk charge sharing model is developed with a two-dimensional charge sharing approach using the sim-

*E-mail: dmkim@kookmin.ac.kr;
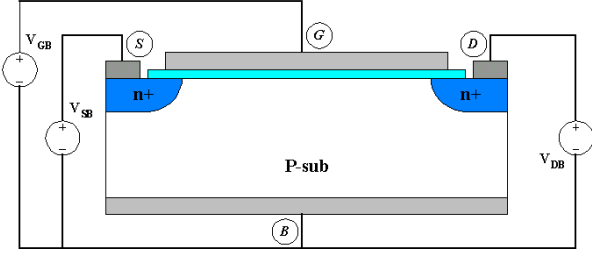Tel: +82-2-910-4719, Fax: +82-2-910-4449

Fig. 1. Cross section of n-MOSFET with terminal voltages referred to body: V_{GB}, V_{DB} and V_{SB}.

ple geometrical approximation in the depletion region in order to express the bulk charge density as a balanced and symmetric function of source- and drain-end surface potentials. We also modeled the channel mobility which is a complicated function of local electric field and position, as an average value of the source- and drain-end channel ones using a balanced bulk charge model. These lead to a simplified and computationally efficient equation for the $I-V$ characteristics and makes possible symmetrical evaluation in both forward ($V_{DS} \geq 0$) and reverse ($V_{DS} \leq 0$) operating modes [6,7].

In the Chapter II, we describe the theoretical aspects of the new $I-V$ model with the bulk charge model, which is described by the balanced bulk charge sharing method, and the averaged surface channel mobility model, which accounts for the physical effect as a combinational function of the transverse and longitudinal electric fields. In the Chapter III, the new model is compared with experimental data measured from n-MOSFETs.

II. CONTINUOUS CHARGE-SHEET MOSFET MODEL FOR CIRCUIT SIMULATION

In contrast to source-referenced model exhibiting discontinuities in the I_{DS} or its derivatives at $V_{DS}=0$, the body-referenced model has been reported to have several advantages with the symmetrical property. Fig. 1 shows the device structure with external terminal voltages. As the symmetry inherent in the body-referenced bias is intellectually satisfying, we proceed to develop a model based on the body-referenced bias such as gate-body (V_{GB}), drain-body (V_{DB}), and source-body (V_{SB}) voltages and will implicitly assume that both source-to-body and drain-to-body junctions are reverse-biased, $V_{DB} \geq 0$, $V_{SB} \geq 0$ [4]. In this chapter, we derive expressions for the continuous and unified charge sheet MOSFET model from subthreshold to strong inversion, from the linear to the saturation regions, and at the boundary between forward and reverse modes of operation.

1. Bulk Charge Model using a Balanced Bulk Charge Sharing Method

The drain current I_D in an n-channel MOSFET is written as

$$I_D = -WQ_i v + WV_{th}\frac{dQ_i}{dy} \qquad (1)$$

where W is the effective channel width, v is the average carrier drift velocity, V_{th} is the thermal voltage, and Q_i represents the inversion charge density. This equation shows that the drain current is the sum of two components, drift and diffusion currents respectively. From Eq. (1), the basis of the charge sheet model is an inversion charge density representation of the intrinsic device between the source and drain boundaries for a structure with a uniform substrate doping concentration and the inversion charge density is a function of the surface potential along the channel. Based on the well-known Poisson equation and charge conservation principles of MOS device physics, the inversion charge density Q_i can be obtained from the difference of the total induced charge Q_s in the channel and the bulk charge Q_b ($Q_i = Q_s - Q_b$) [5]. This can be described as

$$Q_i = -C_{ox}[V_{GB} - V_{fb} - \phi_s] - Q_b, \qquad (2)$$

where V_{GB} is the gate-to-body voltage, V_{fb} is the flat-band voltage, and ϕ_s is the surface potential with respect to the external body-referenced bias. As shown in Eq. (2), the expression for bulk charge density Q_b is important to the overall charge-sheet MOSFET models for simplified and the computationally efficient equation. However, most reported models for bulk charge density Q_b are derived using the source as the reference terminal based on the depletion approximation. Due to this, discontinuities in the derivatives of the drain current and terminal charges appear in the transition region from forward bias to reverse bias operation.

In order to resolve this problem, therefore, we propose a balanced bulk charge density model with respect to surface potential by using an average, position-independent, semi-physical geometrical approximation.

As shown in Fig. 2, we modeled the bulk charge density considering the channel depletion area averaged by the effective channel length. The channel depletion area is geometrically divided into two parts, one associated with the gate and the other associated with the drain and source junction which is similar to the charge sharing concept. The channel depletion area is obtained under assumptions:

- the substrate is uniformly doped N_b.
- the source and drain junctions are cylindrical in shape with a radial junction depth, X_j.
- the channel depletion area is linearized in terms of only source- and drain-end surface potentials.

Thus, from the shaded area under the gate in Fig. 2, the bulk charge density can be obtained. With some physical notation described below,
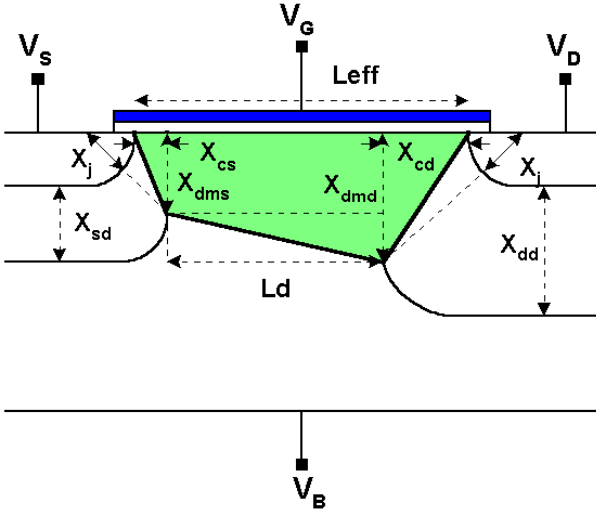
Fig. 2. The balanced charge-sharing model for calculating the bulk charge density as function of surface potentials at source and drain ends.

- the depletion widths of the source to substrate and the drain to substrate, respectively;

$$X_{sd} = \sqrt{\frac{2\epsilon_0\epsilon_{si}}{qN_b}(\phi_{bi} + V_{sb})} \qquad (3)$$

$$X_{dd} = \sqrt{\frac{2\epsilon_0\epsilon_{si}}{qN_b}(\phi_{bi} + V_{db})} \qquad (4)$$

- the built-in potential at the source- and the drain-to substrate junction;

$$\phi_{bi} = \frac{kT}{q}\ln\left(\frac{N_b N_{d,s}}{n_i^2}\right) \qquad (5)$$

- the channel depletion widths at the source- and the drain-end, respectively;

$$X_{dms} = \sqrt{\frac{2\epsilon_0\epsilon_{si}}{qN_b}(\phi_S)} \qquad (6)$$

$$X_{dmd} = \sqrt{\frac{2\epsilon_0\epsilon_{si}}{qN_b}(\phi_D)} \qquad (7)$$

- the lengths of the velocity saturation region at the source and the drain, respectively;

$$X_{cd} = X_j\left(\sqrt{1 + \frac{X_{dmd} + X_{dd}}{X_j}} - 1\right) \qquad (8)$$

$$X_{cs} = X_j\left(\sqrt{1 + \frac{X_{dms} + X_{sd}}{X_j}} - 1\right) \qquad (9)$$

- the length of the gradual channel approximation region;

$$L_d = L_{eff} - (X_{cd} + X_{cs}) \qquad (10)$$

- the total depletion area under gate;

$$A_{dm} = \frac{1}{2}L_d(X_{dmd} + X_{dms}) + \frac{1}{2}(X_{cs}X_{dms} + X_{cd}X_{dmd}) \qquad (11)$$

Therefore, the bulk charge per unit area can be obtained from

$$Q_{BBC} = -qN_b\frac{A_{dm}}{L_{eff}} \qquad (12)$$

which is the total bulk charge ($qN_b A_{dm}$) averaged by the effective channel length (L_{eff}). Above all, to be able to calculate the bulk charge density from Eq. (12) the surface potential at the source and drain ends need to be evaluated. For given values of V_{GB} and V_{SB} or V_{DB}, the surface potential (ϕ_s) can be obtained using an iterative numerical approach with

$$\phi_s(x) = V_{GB} - V_{fb} + \phi_s - \gamma\sqrt{\phi_s + V_{th}e^{-\phi_s/V_{th}} + e^{(-2\phi_f - V_{CB})/V_{th}}\{V_{th}e^{\phi_s/V_{th}} - \phi_s e^{V_{CB}/V_{th}} - V_{th}\}} \qquad (13)$$

$$\phi_S(x \equiv 0) = V_{GB} - V_{fb} - \gamma\sqrt{\phi_S + V_{th}e^{(\phi_S - 2\phi_f - V_{SB})/V_{th}}} \qquad (14)$$

$$\phi_D(x \equiv L_{eff}) = V_{GB} - V_{fb} - \gamma\sqrt{\phi_D + V_{th}e^{(\phi_D - 2\phi_f - V_{DB})/V_{th}}}. \qquad (15)$$

Eq. (13) is a implicit equation in surface potential derived by solving Poisson's equation in the surface region and Eqs. (14)-(15) are simplified expressions beyond inversion state. Once surface potential is determined, the bulk charge density can be obtained easily by inserting

Eqs. (14)-(15) into Eq. (12). The inversion charge density can be re-described by

$$Q_i = -C_{ox}\left(V_{GB} - V_{FB} - \phi_s - \frac{qN_b}{C_{ox}}\frac{A_{dm}}{L_{eff}}\right). \qquad (16)$$
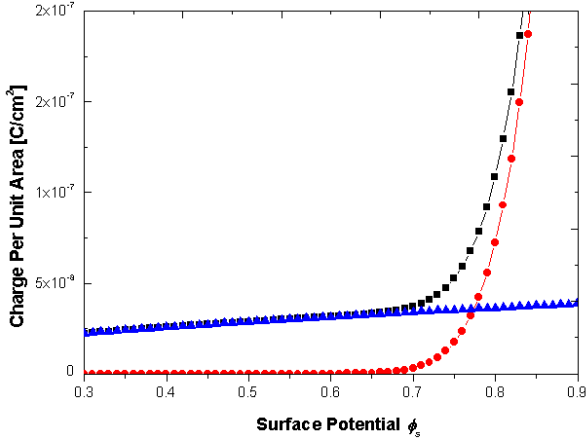
Fig. 3. Variation of inversion charge density $Q_i(\bigcirc)$, bulk charge density $Q_b(\triangle)$, and the total charge density $Q_s(\square)$ ($Q_s=Q_i+Q_b$) versus the surface potential ϕ_s in all regimes of device operation for a p-type substrate with $N_b=5\times10^{15}$ cm^{-3} and $T_{ox}=300$ Å.

In order to verify a new bulk charge model using a BBCS method, Fig. 3 shows the comparative results of the inversion charge density (Q_i), bulk charge density (Q_b), and total induced charge density (Q_s) as a function of surface potential with a conventional charge density model [5] for a p-type substrate, $N_b=5\times10^{15}$ cm^{-3}, oxide thickness, $T_{ox}=300$ Å, and flatband voltage, $V_{fb}=0$ V.

2. Improved Surface Channel Mobility Model

Surface channel mobility is one of the most important parameters in modeling the $I-V$ characteristics of modern MOSFETs. For compact mobility modeling, it is well known that the effective mobility is solely a function of the effective transverse field (ϵ_{eff}) and described by [11, 12]

$$\mu_{eff} = \frac{\mu_0}{1 + \left(\frac{\epsilon_{eff}}{\epsilon_0}\right)} \quad (17)$$

$$\epsilon_{eff} = \frac{Q_b + Q_i/2}{\epsilon_{si}} \quad (18)$$

where ϵ_0 is the critical field, v is a fitting parameter, and ϵ_{eff} is the average electric field experienced by the carriers in the inversion layer. In Eq. (18), the average electric field is a function of the inversion charge and bulk charge density. Therefore, in order to include the influence of the lateral electric field and the position-independent characteristic along the channel, we insert Eq. (12) and Eq. (16) into Eq. (18), and the inversion charge density is substituted by the average inversion charge density, $Q_{i,avg} = (Q_{iS} + Q_{iD})/2$, where Q_{iS} and Q_{iD} are the inversion charge densities at the source and drain end, respectively, as a function of ϕ_S and ϕ_D from

Eqs. (14)-(15). Then, the average electric field over the channel is re-described as

$$\epsilon_{eff,avg} = \frac{Q_b + 0.5Q_{i,avg}}{\epsilon_{si}}$$
$$= \left(V_{GB} - V_{fb} - \frac{(\phi_S + \phi_D)}{2} + \frac{qN_b}{C_{ox}}\frac{A_{dm}}{L_{eff}}\right)/6T_{ox}. \quad (19)$$

It is important that Eq. (19) expresses the effective electric field as a balanced symmetric equation for the source- and drain-end potentials. This is another efficient solution for improving the discontinuity problem in $I-V$ characteristics at the forward and reverse operation boundary. As a result, we have

$$\mu_{eff,avg} = \frac{\mu_0}{1} + U_c V_{BP}$$
$$\times \left(0.5(V_{GB} - V_{GT}) + \frac{U_a V_{BP}}{6}T_{ox} \times 10^6\right)^n \quad (20)$$

where the μ_0 is the maximum extracted value of the mobility, V_{BP} and V_{GT} in new model are defined by

$$V_{BP} = \frac{qN_b}{C_{ox}}\frac{A_{dm}}{L_{eff}} \quad (21)$$

$$V_{GT} = V_{fb} + \frac{\frac{(\phi_S}{\phi_D)}}{2} + V_{BP}g \quad (22)$$

The term $U_c V_{BP}$ is introduced to improve the model accuracy at high body bias [2] and U_a, U_c and n are parameters to be determined by fitting to the experimental $I-V$ data.

3. Continuous Current-Voltage Characteristics of MOSFETs

In this section, we show that a continuous and unified MOSFET model can be effectively developed with the help of the average, position independent, bulk charge density and the surface channel mobility model, including the most important physical effects such as velocity saturation, output conductance modulation, and drain induced barrier lowering (DIBL). When the diffusion current is neglected from Eq. (1), the drift current is rewritten as

$$I_{drift} = -WQ_iv. \quad (23)$$

Next, most commonly used velocity-field ($v-E$) expression for a variation of the carrier velocity with lateral electric field is chosen as [5]

$$v = \frac{\mu_{eff}(d\phi_s/dy)}{\left\{1 + \left(\frac{\mu_{eff}}{v_{sat}}\frac{d\phi_s}{dy}\right)^\beta\right\}^{1/\beta}} \quad (24)$$

where μ_{eff} is an effective mobility, v_{sat} is the saturation velocity, β is an empirical fitting parameter, and $d\phi_s/dy$ is the lateral field. Eq. (24) is inserted in Eq. (23), both sides of the equation are rearranged, and integrating both sides under the boundary condition as

$$\phi_s = \begin{cases} \phi_S & at \ y = 0 \\ \phi_D & at \ y = L_d \end{cases} \tag{25}$$

where the L_d is defined by $L_d = L_{eff} - (X_{cd} + X_{cs})$. As seen from Fig. 2, the channel can be divided into three regions, the source channel junction of length X_{cs}, the drain channel junction of length X_{cd}, and the linear region of length L_d. The resulting equation is expressed by

$$I_{drift}(y) = -WQ_i v$$
$$= -\frac{WQ_i \mu_{eff}(d\phi_s/dy)}{\left\{1 + [(\mu_{eff}d\phi_s/dy)/v_{sat}]^\beta\right\}^{1/\beta}} \tag{26}$$

$$I_{drift} \int_0^{L_d} \left[\frac{\{1 + [(\mu_{eff}d\phi_s/dy)/v_{sat}]^\beta\}^{1/\beta}}{\mu_{eff}}\right] dy$$
$$= W \int_{\phi_S}^{\phi_D} Q_i d\phi_s \tag{27}$$

$$I_{drift} \frac{\left\{1 + \left(\frac{\mu_{eff,avg}}{v_{sat}}\frac{(\phi_D - \phi_S)}{L_d}\right)^\beta\right\}^{1/\beta}}{\mu_{eff,avg}} L_d$$
$$= WC_{ox} \int_{\phi_S}^{\phi_D} (V_{GB} - V_{fb} - \phi_s - V_{BP})d\phi_s. \tag{28}$$

In the derivation of Eq. (28) for Eq. (27), the effective mobility μ_{eff} is substituted by the average effective mobility $\mu_{eff,avg}$ and the term $d\phi_s/dy$ is replaced by the average lateral electric field $(\phi_D - \phi_S)/L_d$ in the linear region. Then, the left-hand side of Eq. (27) has been integrated and obtained Eq. (28). Also, the right-hand side of Eq. (27) is substituted by the inversion charge density, Eq. (16), with the average bulk charge density Eq. (12). This leads to simplified and computationally efficient equation of the continuous current voltage characteristic of MOSFET model. Also, the right-hand side of Eq. (28) can be integrated with the contribution of the average bulk charge density and the resultant drift current is expressed as

$$I_{drift} = \mu_{eff,avg}C_{ox}\left(\frac{W}{L_d}\right)$$
$$\times \frac{(V_{GB} - V_{fb} - V_{BP})(\phi_D - \phi_S) - \frac{1}{2}(\phi_D^2 - \phi_S^2)}{\left\{1 + \left(\frac{\mu_{eff,avg}}{v_{sat}}\frac{(\phi_D - \phi_S)}{L_d}\right)^\beta\right\}^{1/\beta}}. \tag{29}$$

While the drift current is a dominant component in the strong-inversion mode, the diffusion current is dominant

in the subthreshold region. Both drift and diffusion components should be considered in the moderate-inversion region. Therefore, the diffusion current still needs to be evaluated and given as

$$I_{drift} = W\mu_{eff}V_{th}\frac{dQ_i}{dy}. \tag{30}$$

In the same process for drift current, both sides can be integrated under the boundary condition, Eq. (25), as

$$\frac{I_{drift}}{\mu_{eff}}dy = WV_{th}dQ_i \tag{31}$$

$$\int_0^{L_d} \frac{I_{drift}}{\mu_{eff}}dy = WV_{th}\int_{Q_{iD}}^{Q_{iS}} dQ_i = \int_{\phi_D}^{\phi_S} d\phi_s \frac{dQ_i}{d\phi_s}. \tag{32}$$

However, in Eq. (26), Q_i cannot be differentiated with the surface potential due to the averaged bulk charge density. For the reason, we put the condition of $Q_b = \gamma C_{ox}\sqrt{\phi_s} = qN_b A_{dm}/L_{eff}$ into Eq. (16) as following

$$Q_i = C_{ox}\left(V_{GB} - V_{fb} - \phi_s - \frac{qN_b}{C_{ox}}\frac{A_{dm}}{L_{eff}}\right)$$
$$= C_{ox}(V_{GB} - V_{fb} - \phi_s - \gamma\sqrt{\phi_s}). \tag{33}$$

Inserting Eq. (33) into the right-hand side of Eq. (32), the inversion charge density (Q_i) can be differentiated with the surface potential (ϕ_s). Then, the averaged bulk charge density is reused as the following

$$\frac{dQ_i}{d\phi_s} = C_{ox}\left(-1 - \frac{\gamma}{2\sqrt{\phi_s}}\right)$$
$$= C_{ox}\left(-1 - \frac{\gamma^2 C_{ox}}{2qN_b A_{dm}/L_{eff}}\right)$$
$$= -C_{ox}\left(1 + \frac{\gamma^2}{V_{BP}}\right) \tag{34}$$

where

$$\gamma = \frac{\sqrt{2\epsilon_0\epsilon_{si}qN_b}}{C_{ox}}. \tag{35}$$

As a result, Eq. (32) is integrated with a surface potential (ϕ_s) due to the average bulk charge density as following equation

$$I_{drift} = \mu_{eff,avg}C_{ox}\left(\frac{W}{L_d}\right)V_{th}\left(1 + \frac{\gamma^2}{V_{BP}}\right)(\phi_D - \phi_S). \tag{36}$$

In order to obtain a unified channel charge model which is continuous and accurate from subthreshold to strong inversion regions, the drift current, Eq. (29) and diffusion current, Eq. (36) can be combined to model the drain current as

$$I_{DS} = \mu_{eff,avg}C_{ox}\left(\frac{W}{L_d}\right)\frac{(V_{GB} - V_{GT})(\phi_D - \phi_S) + V_{th}\left(1 + \frac{\gamma^2}{V_{BP}}\right)(\phi_D - \phi_S)}{\left\{1 + \left(\frac{\mu_{eff,avg}}{v_{sat}}\frac{(\phi_D-\phi_S)}{L_d}\right)^{\beta}\right\}^{1/\beta}}. \tag{37}$$
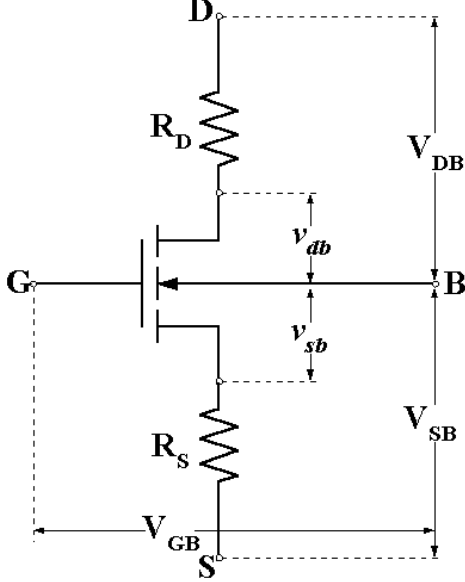

Fig. 4. MOSFET showing internal and external terminal voltages when the source and drain resistances (R_S and R_D) are taken into account.

4. Parasitic Source and Drain Resistance Effect in the $I - V$ Model

As was pointed out earlier, the scaling down of MOS-FETs to deep submicrometer regimes leads to departures from assumptions made by simplifying $I - V$ model [5]. From one of the assumptions, the voltage drops across the series resistances R_S and R_D associated with the source and drain regions, respectively, are negligible compared to the applied voltages. It is therefore important to model these elements in order to simulate the device behavior accurately. The schematic diagram of the voltage drop pattern in the extrinsic and intrinsic regions is shown in Fig. 4.

We assume that the series resistances R_S and R_D are

independent of the bias. When the intrinsic drain-to-body and source-to-body voltages are denoted by V_{db} and V_{sb} respectively, from Kirchiff's law, expressed as

$$V_{db} = V_{DB} - I_D R_D, \tag{38}$$

$$V_{sb} = V_{SB} + I_D R_S. \tag{39}$$

and the external terminal drain- and source-to-body voltage is replaced with intrinsic drain- and source-to-body voltages into the surface potential Eqs. (14)-(15) as

$$\begin{aligned}\phi_S &= V_{GB} - V_{fb} - \gamma\sqrt{\phi_S + V_{th}e^{(\phi_S - 2\phi_f - V_{sb})/V_{th}}}\\\phi_D &= V_{GB} - V_{fb} - \gamma\sqrt{\phi_D + V_{th}e^{(\phi_D - 2\phi_f - V_{db})/V_{th}}}.\end{aligned} \tag{40}$$

As the end, to calculate the electric boundary continuous between linear and saturation regions, we must take into account the limitation of the inversion charge density at the drain region due to the velocity saturation. When the drain voltage is so large enough that the carrier velocity is reached the saturation velocity v_{sat}, the inversion charge density at the drain region is pinned at a constant value. That is, with a fixed gate bias, as the drain voltage is increased, the inversion charge density at the drain region decreases. Also, as the inversion charge density at the drain region decreases, the potential across the channel must be adjusted to increase the carrier velocity at the drain region so that the drain current is maintained corresponding to this condition. At this point, while the velocity saturation behavior for a variation of the carrier velocity with lateral electric field is modeled using the smoothing function Eq. (24), the reduction of the inversion charge density for a variation of the carrier velocity with lateral electric field is not considered. So, we included this behavior into Eq. (37) to satisfy the necessary smoothness between the linear and saturation regimes as following

$$I_{DS} = \mu_{eff,avg}C_{ox}\left(\frac{W}{L_d}\right)\frac{\{V_{GB} - V_{GT} - \kappa(\phi_D - \phi_S)\}(\phi_D - \phi_S) + V_{th}\left(1 + \frac{\gamma^2}{V_{BP}}\right)(\phi_D - \phi_S)}{\left\{1 + \left(\frac{\mu_{eff,avg}}{v_{sat}}\frac{(\phi_D-\phi_S)}{L_d}\right)^{\beta}\right\}^{1/\beta}} \tag{41}$$

where κ is a fitting parameter used to better adjust the curvature of the transition from linear to saturation

regimes. For completeness, it is noted that the smoothing parameters β and κ are fitted simultaneously due to
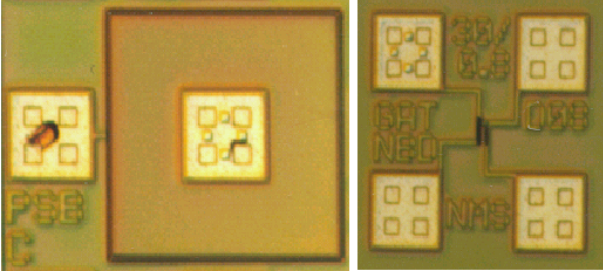
Fig. 5. Layout and probe pad structure of a Si-MOS Capacitor with $W \times L$=300×300 μm^2 and a Si-MOSFETs with W/L=30 μm/0.6 μm fabricated on a p-type silicon wafer using a standard CMOS process.

Table 1. Extracted Model parameters in n-MOSFET (W/L=30 μm/0.6 μm).

Symbols in equation	Extraction value	Unit
C_{ox}	153	pF
T_{ox}	220	Å
N_b	$6.65 \cdot 10^{16}$	cm^{-3}
X_j	0.08	μm
V_{GT}	0.54	V
V_{fb}	-1.07	V
ΔL	0.21	μm
R_D	18.48	Ω
R_S	17.85	Ω
μ_0	675	cm^2/V·sec
U_a	0.12	–
U_c	6.39	–
v_{sat}	$8 \cdot 10^4$	m/sec
β	1.84	–
κ	0.6	–

the dependency of the same physical source.

III. SIMULATION RESULTS AND EXPERIMENTAL VERIFICATION

For the verification of the proposed charge sheet model in the paper, we extracted characteristic parameters for the BBCS model [13–16]. The measurement system consists of HP 4284A LCR meter and HP 4145B semiconductor parameter analyzer under the control of a desktop computer. Fig. 5 shows 300×300 μm^2 MOS capacitor and MOSFETs with gate length L=0.6 μm and gate width W=30 μm fabricated on a p-type silicon wafer using a standard CMOS process.

Experimentally observed typical current-voltage characteristics of n-channel Si MOSFETs with W=30 μm and L=0.6 μm are shown in Fig. 6 and all extracted parameter values are arranged in Table 1.
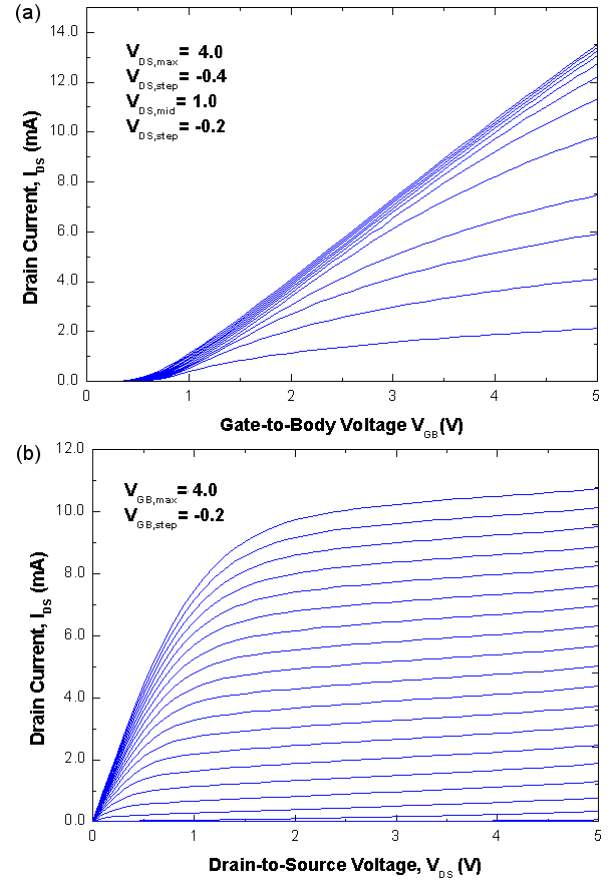

Fig. 6. $I - V$ characteristics for Si-MOSFETs with W=30 μm and L=0.6 μm : (a) Drain current vs. Gate-to-Body Voltage characteristics. (b) Drain current vs. Drain-to-Source Voltage characteristics.

1. $I - V$ Characteristics for the Continuous Charge-Sheet Model

Fig. 7 shows the measured and modeled input characteristics of n-channel MOSFETs with W=30 μm and L=0.6 μm. The agreement between the modeled and experimental data is satisfactory for the measurement results and the theoretical calculation all over the regions from linear to saturation of the drain biases. We also show the output characteristics of the same n-channel MOSFET in Fig. 8. The solid lines are the modeled results and the circle lines are the measured data. The fitted results are very good for the same model parameters shown in Table 1. This result means that the proposed model is very accurate and suitable for submicrometer MOSFETs. Since the smoothing parameters for the velocity saturation and inversion charge pinning effect at the drain region are fitted simultaneously, the output characteristics shows no discontinuity at the boundary between the linear and saturation regions. In Fig. 9, the drain current versus gate-to-body voltage is shown on a linear scale to demonstrate the unified characteristics
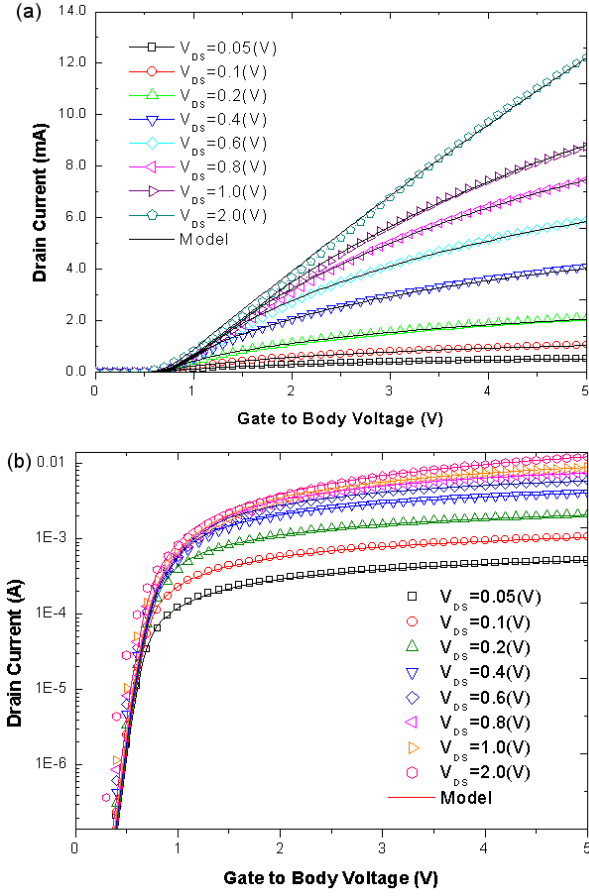
Fig. 7. I_{DS}-V_{GS} characteristics from linear region to saturation region for an n-channel MOSFET with W=30 μm and L=0.6 μm at different drain biases $V_{DS}(V_{DB}$-$V_{SB})$. (a) I_{DS}-V_{GS} characteristics in a linear scale. (b) I_{DS}-V_{GS} characteristics in a logarithmic scale.

Fig. 8. I_{DS}-V_{DS} characteristics of the device with W/L=30 μm/0.6 μm at different gate-to-body bias V_{GB}. (a) Measured and modeled I_{DS}-V_{DS} characteristics in linear scale. (b) Measured and modeled G_{DS}-V_{DS} characteristics in logarithmic scale.

in the proposed model. We also show the comparison results in Fig. 8(b) and Fig. 9(b) for the g_m and g_{ds} through the experimental data and modeled electrical characteristics which are a sensitive test for the accuracy of the model. Fig. 10 shows the drain current versus the gate-to-source voltage (V_{GB}-V_{SB}) at different body biases on a logarithmic scale to demonstrate the characteristics in the subthreshold region. From this figure, it can be seen that the model accurately describes a shift in the threshold voltage with the body bias.

2. Result of Gummel Symmetry Test

Most of the well-known problems with conventional $I - V$ models for MOSFETs were related to discontinuities in the conductance at the boundary between linear and saturation regions or at the boundary between weak and strong inversion conditions. These problems have been solved quite successfully by utilizing a unified
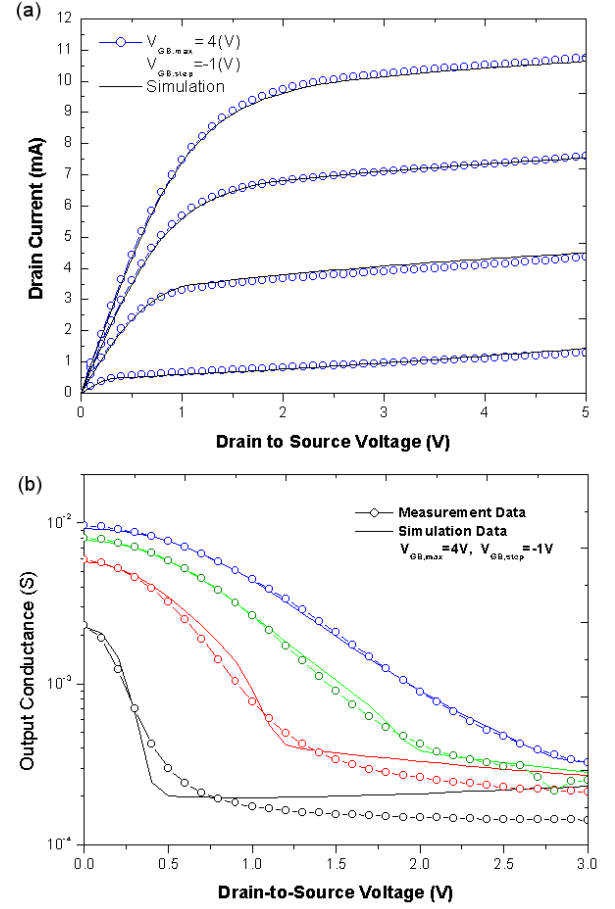
modeling of the drain currents in all regions of operating biases. However, the other attention has been given to maintaining continuity in the charge and current models exclusively in the forward or reverse regions. Therefore, the charge-sheet model based on the symmetric linearisation must pass the Gummel symmetry test [6,7,11]. At V_{DS} 0V operating point, the Gummel symmetry test can be used to demonstrate the common problems in most compact MOSFET models.

As shown in Fig. 11, this test uses the circuit that drives a MOSFET symmetrically in both forward and reverse modes by sweeping only one source with the gate-substrate bias fixed at V_{GBO}. Since the source-to-body bias is $V_{BO} - V_X$ and the drain-to-body bias is $V_{BO} + V_X$ with the initial nonzero source-to-substrate bias, V_{BO} and an independent voltage source, V_X, V_{DS} ($V_{DB} - V_{SB}$) is always equal to $2V_X$. If V_X is swept from a negative value to an equal positive value, the transistor under test is driven symmetrically from a reverse mode to a forward mode. Further, if drain current and
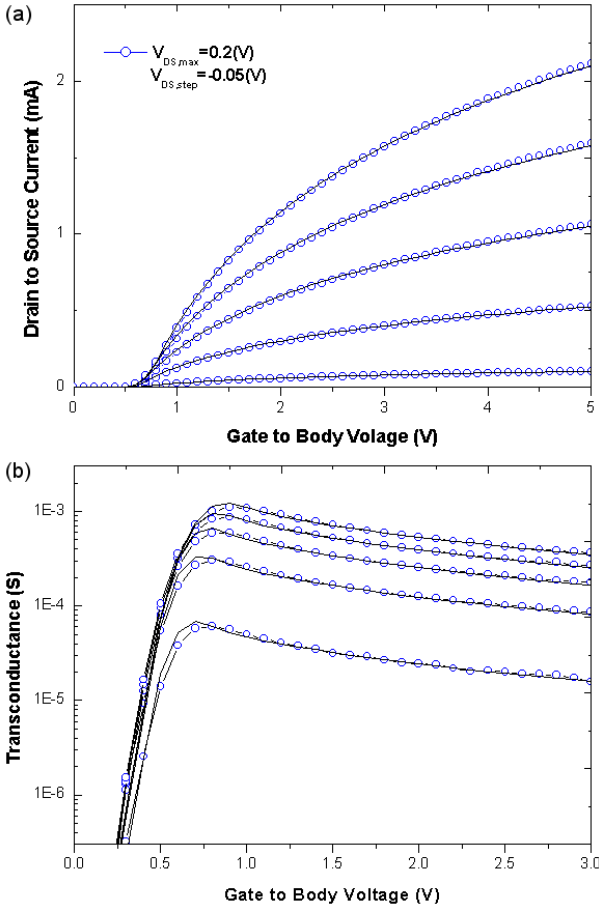
(a)

(b)

Fig. 9. I_{DS}-V_{GS} characteristics in linear region for an n-channel MOSFET with W=30 μm and L=0.6 μm at different drain biases V_{DS}(=V_{DB}-V_{SB}). (a) Measured and modeled I_{DS}-V_{GS} characteristics (b) Measured and modeled G_m-V_{GS} characteristics in logarithmic scale.
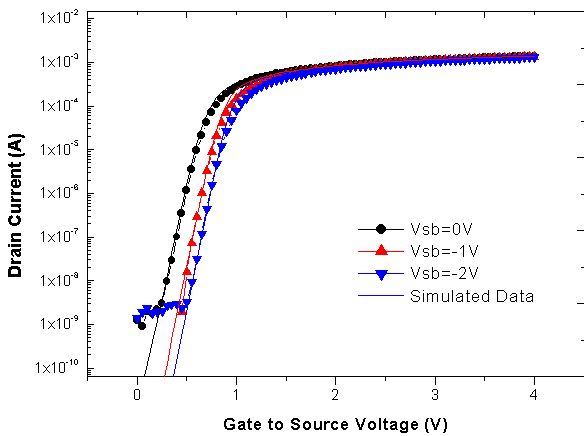

Fig. 10. A comparison of measured and simulated drain current in the linear region for an n-channel MOSFET with W=30 μm, L=0.6 μm at different body biases.

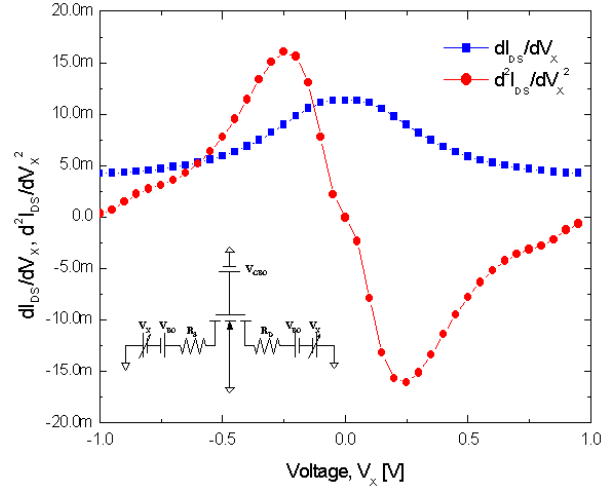all its higher-order derivatives with respect to the ter-

Fig. 11. Results of Gummel symmetry test: Plots of dI_D/dV_X and d^2I_D/dV_X^2 obtained from a simulation using the new BBCS model under V_{GBO}=3 V.

minal voltages are continuous, it implies that the second derivative of drain current with respect to V_X should also be equal to zero at V_X=0. As shown in Figure 11, the continuous charge-sheet model using the BBCS method discussed in this paper passes the Gummel symmetry test.

IV. CONCLUSION

In this thesis, the concept of a balanced bulk charge sharing (BBCS) method is used to build a new analytical charge sheet MOSFET model for analog/digital circuit simulation. The comparisons between the model and measured data in n-channel MOSFETs show that the proposed model can describe the $I - V$ characteristics accurately and smoothly from a subthreshold to a strong inversion in the gate bias as well as from the linear to the saturation regions in the drain bias. In particular, discontinuities in the second derivative in other conventional MOSFET models at the electrical boundary between forward and reverse mode operations have been eliminated by averaging the bulk charge and mobility over the channel length with respect to the function of the source and drain end surface potentials. In addition, the resulting MOSFET model satisfies the Gummel symmetry test. With results in this paper, we can expect that the new model can be easily implemented in circuit simulators for VLSI design.

ACKNOWLEDGMENTS

REFERENCES

[1] Y. Cheng, M. C. Jeng, Z. Liu, J. Huang, M. Chan, K. Chen, P. K. Ko and C. Hu, IEEE Trans. Electron Dev. **44**, 277 (1997).

[2] Y. Cheng and C. Hu, *MOSFET Modeling & BSIM3 User's Guide* (Kluwer Acadmic Publishers, Boston, 1999).

[3] Y. Cheng, K. Chen, K. Imai and C. Hu, IEEE Trans. Electron Dev. **17**, 641 (1998).

[4] Y. P. Tsividis, *Operation and Modeling of the MOS Transistor* (McGraw-Hill, New York, 1999).

[5] N. Arora, *MOSFET Models for VLSI Circuit Simulation Theory and Practice* (Springer-Verlag Wien, New York, 1993).

[6] Y. P. Tsividis and K. Suyama, IEEE J. Solid-State Circuits **SC-29**, 210 (1994).

[7] K. Joarkar, K. K. Gullapalli, C. C. McAndrew, M. E. Burnham and A. Wild, IEEE Electron Dev. **45**, 134 (1998).

[8] K.-H. Baek, G. M. Lim, S. D. Cho, Y. C. Kim, H. C. Kim, S. K. Kim, D. J. Kim and D. M. Kim, J. Korean Phys. Soc. **37**, 915 (2000).

[9] M. K. Won, C. Choi, C. An, M. S. Kang and Y. S. Koo, J. Korean Phys. Soc. **39**, S170 (2001).

[10] Y. C. Kim, H. T. Kim, S. D. Cho, S. J. Song, S. S. Chi, H. C. Kim, S. K. Kim, K. H. Baek, G. M. Lim, D. J. Kim and D. M. Kim, J. Korean Phys. Soc. **40**, 60 (2002).

[11] T. L. Chen and G. Gildenblat, Electronics Lett. 7th **37**, 791 (2001).

[12] S. C. Sun and D. Plummer, IEEE J. Solid-State Circuits **SC-45**, 562 (1990).

[13] L. Selmi, E. Sangiorgi and B. Ricco, IEEE Trans. Electron Dev. **36**, 1094 (1989).

[14] B.-J. Moon, C.-K. Park, K. Lee and M. Shur, IEEE Trans. Electron Dev. **38**, 592 (1991).

[15] G. M. Lim, Y. C. Kim, D. J. Kim, Y. W. Park and D. M. Kim, Electronics Lett. 6th **36**, 1233 (2000).

[16] K. Chen, H. C. Wann, J. Dunster, P. K. Ko, C. Hu, Solid-State Electronics **39**, 1515 (1996).